

Resonant inelastic x-ray scattering study of the spin and charge excitations in the overdoped superconductor $\text{La}_{1.77}\text{Sr}_{0.23}\text{CuO}_4$

C. Monney,^{1,2} T. Schmitt,¹ C. E. Matt,^{1,3} J. Mesot,^{1,4,3} V. N. Strocov,¹ O. J. Lipscombe,⁵ S. M. Hayden,⁵ and J. Chang^{1,4,2}

¹*Paul Scherrer Institut, Swiss Light Source, CH-5232 Villigen PSI, Switzerland*

²*Physik-Institut, Universität Zürich, Winterthurerstrasse 190, CH-8057 Zürich, Switzerland*

³*Laboratory for Solid State Physics, ETH Zürich, CH-8093 Zürich, Switzerland*

⁴*Institute for Condensed Matter Physics, École Polytechnique Fédérale de Lausanne (EPFL), CH-1015 Lausanne, Switzerland*

⁵*H. H. Wills Physics Laboratory, University of Bristol, Bristol BS8 ITL, United Kingdom*

(Received 16 October 2015; revised manuscript received 22 December 2015; published 1 February 2016)

We present a resonant inelastic x-ray scattering (RIXS) study of spin and charge excitations in overdoped $\text{La}_{1.77}\text{Sr}_{0.23}\text{CuO}_4$ along two high-symmetry directions. The line shape of these excitations is analyzed and they are shown to be highly overdamped. Their spectral weight and damping are found to be strongly momentum dependent. Qualitative agreement between these observations and a calculated random-phase approximation susceptibility is obtained for this overdoped compound, implying that a significant contribution to the RIXS signal stems from a continuum of charge excitations. Furthermore, this suggests that the spin excitations in the overdoped regime can be captured qualitatively by an itinerant picture. Our calculations also predict a low-energy spin-excitation branch to exist along the nodal direction near the zone center. With the energy resolution of the present experiment, this branch is not resolvable, but we show that the next generation of high-resolution spectrometers will be able to test this prediction.

DOI: 10.1103/PhysRevB.93.075103

I. INTRODUCTION

Conventional superconductivity emerges as a result of electron-phonon interaction [1]. Information about the phonon excitation spectrum (dispersions and lifetime effects [2]) is therefore of great importance. Similarly, for magnetic superconductors [3], there is a strong interest in understanding and experimentally revealing the spin-excitation spectrum. Mapping out the detailed evolution of the spin-excitation spectrum across the high-temperature superconducting cuprate phase diagram, from the Mott insulator to the Fermi-liquid ground state, is hence important. Spin excitations have traditionally been studied by inelastic neutron scattering (INS) [4,5]. Studies of high-energy spin excitations [6] have, however, been challenged by weak neutron cross sections. Over the last decade, resonant inelastic x-ray scattering (RIXS) has developed rapidly [7] and energy resolution now allows studies of spin excitations [8–10]. RIXS is therefore an attractive complementary technique to neutron scattering. This has, in particular, lead to progress in understanding correlated low-dimensional $3d$, $4d$, and $5d$ electron systems [11–13]. The spin-excitation spectra of insulating one- and two-dimensional cuprates have, for example, been studied by soft x-ray RIXS using the copper L_3 edge [12,14–19]. In recent years, spin excitations of doped cuprate and pnictide superconductors have also been investigated [9,10,12,20]. These studies suggest that the high-energy ($\omega > 100$ meV) spin-excitation dispersion undergoes little change with doping [12,20,21]. This is in strong contrast to the low-energy part of the spectrum (studied by INS), which has a strong dependence on impurities [22], magnetic field [23,24], and doping [25,26].

We present a systematic RIXS study of the spin and charge excitations found in overdoped $\text{La}_{2-x}\text{Sr}_x\text{CuO}_4$ (LSCO), $x = 0.23$. The line shape of these excitations is analyzed using the response function of a damped harmonic oscillator. In this fashion, their dispersion and momentum dependence of

spectral weight and damping γ are extracted. We find that the spectral weight and damping γ display a significant momentum dependence. The line shape is sharpest around the zone center, whereas the spectral weight increases upon moving towards the zone boundary. As reported for Bi-based cuprates [16,27], we also find a strong nodal/antinodal anisotropy of spectral weight. These observations are captured by susceptibility calculations based on the electronic band structure. The model calculation furthermore predicts a low-energy spin-excitation branch, along the (π,π) direction, which turns out to be particularly pronounced and dispersive in LSCO with $x = 0.23$ in comparison to other doped cuprates [16,28]. Future RIXS experiments with improved energy resolution should test this prediction.

II. METHOD

High-resolution RIXS experiments were carried out at the Advanced Resonant Spectroscopy (ADRESS) beam line [29,30] at the Swiss Light Source (SLS) on high-quality single-crystalline LSCO $x = 0.23$ samples [26,31–33], grown by the traveling floating zone method [34]. For the tetragonal crystal structure ($a = b \approx 3.8$ Å and $c \approx 13.2$ Å), we index the reciprocal space by $q = h\mathbf{a}^* + k\mathbf{b}^* + \ell\mathbf{c}^*$, where \mathbf{a}^* and \mathbf{b}^* point along the Cu-O bonds. Samples were aligned *ex situ*, using the x-ray Laue technique, in order to access the scattering planes $(h,0,\ell)$ or (h,h,ℓ) . Cleaving was performed *in situ* under ultrahigh-vacuum conditions ($< 5 \times 10^{-10}$ mbar) using a standard top-post technique and the sample was kept at a temperature of 20 K for all measurements. At the Cu L_3 edge (~ 930 eV), the instrumental energy and momentum half width at half maximum (HWHM) resolutions are 65 meV and 0.01 Å⁻¹, respectively. The incoming light was σ polarized for all measurements. For each spectrum, the elastic line was obtained by measuring nonresonant elastic scattering from

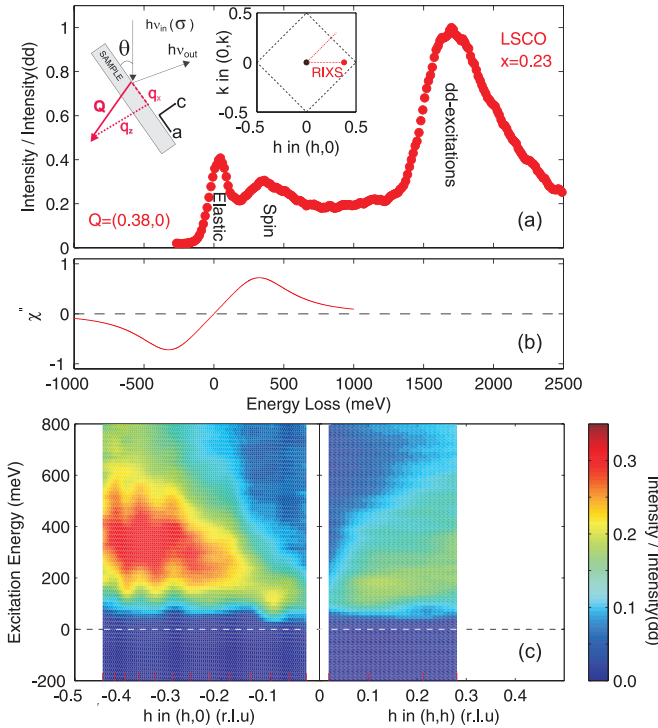


FIG. 1. (a) RIXS spectrum, recorded on overdoped LSCO $x = 0.23$ using σ -polarized light, displays elastic scattering, a low-energy excitation, and a dd excitation. The inset shows the scattering geometry and reciprocal space (h, k) schematically. (b) Overdamped response function showing how $\chi'' \rightarrow 0$ for $\omega \rightarrow 0$. (c) Interpolated RIXS intensity, with elastic scattering subtracted, vs momentum $q = (h, 0)$, (h, h) and photon energy loss ω . Red ticks indicate the grid of the spectra used for the interpolation.

polycrystalline carbon containing tape placed just next to the sample [15]. Reciprocal space positions of the form $(h, 0, \ell)$ and (h, h, ℓ) were sampled by changing the grazing incident angle θ , defined in Fig. 1. The layered cuprates are known to have weak magnetic coupling along the c axis, leading to little dispersion along ℓ . We therefore describe positions using a two-dimensional notation (h, k) to quantify momentum transfer q .

III. RESULTS

A typical RIXS spectrum recorded with σ -polarized light at $(h, k) = (0.38, 0)$ is shown in Fig. 1(a). As previously reported on the cuprates [10,12,28], the spectrum consists of three features: (1) elastic and quasielastic scattering at $\omega \approx 0$, (2) a low-energy excitation at around 300 meV that has been interpreted as a spin excitation in the parent compound [9,10], and (3) so-called dd excitations at about 1700 meV. The dd excitations are in agreement with what has previously been reported on LSCO [35] and explained by crystal field calculations [36,37]. Following common practice, all spectral intensities are renormalized to total integrated intensity of these dd excitations, I_{dd} [21,28,38].

As expected, significant elastic scattering is found near the specular condition [$q = (0, 0)$]; see Fig. 2(a). The increased elastic scattering near the grazing incidence condition

$q \approx (0.4, 0)$ was previously interpreted as a result of a phonon branch [10]. Herein, we make no attempt to disentangle contributions from phonons and elastic scattering. We also stress that contrary to what was reported [10] in underdoped LSCO $x = 0.08$, only one low-energy excitation branch is resolved in our RIXS spectra of overdoped LSCO. Hence, there is no evidence for phase separation in our compound.

A systematic compilation of RIXS spectra taken along the $(h, 0)$ and (h, h) directions is shown in Fig. 2. For simplicity, only the elastic scattering and low-energy excitations are shown. In Fig. 1(c), the spectral weight originating from these excitations is displayed using a false color scale and after subtracting the elastic component. Without any detailed analysis, the following observations can be made. (1) Although weaker, their spectral weight remains finite in the region near the zone center $q = (0, 0)$; see Fig. 1(c). (2) The spectral weight is weaker and the excitations broader and less dispersive along the (h, h) direction. A similar dichotomy between “nodal” (h, h) and “antinodal” $(h, 0)$ directions has also been reported for optimally and underdoped $\text{Bi}_2\text{Sr}_2\text{CaCu}_2\text{O}_{8+\delta}$ [16,27] (Bi2212). The less dispersive nodal excitation has also been reported for overdoped LSCO ($x = 0.25$) [39].

IV. ANALYSIS

A. Data modeling

To model the spectral weight from elastic and low-energy scattering, we use the formula $\frac{I}{I_{dd}}(\omega) = G(\omega) + n_B \chi''(\omega)$, where $n_B = [1 - \exp(\hbar\omega/k_B T)]^{-1}$ accounts for the Bose factor. $G(\omega)$ is a Gaussian function (to fit the elastic line) on top of a background modeled by a cubic polynomial. The response function $\chi''(\omega)$ is that of a damped harmonic oscillator:

$$\begin{aligned} \chi''(\omega) &= \chi_0'' \frac{\gamma\omega}{[\omega^2 - \omega_0^2]^2 + \omega^2\gamma^2} \\ &= \frac{\chi_0''}{2\omega_1} \left[\frac{\gamma/2}{(\omega - \omega_1)^2 + (\gamma/2)^2} - \frac{\gamma/2}{(\omega + \omega_1)^2 + (\gamma/2)^2} \right], \end{aligned}$$

where the damping coefficient $\gamma/2 = \sqrt{\omega_0^2 - \omega_1^2}$. Considering for a moment only magnetic excitations, this response function spans two conceptually different regimes. In the limit $\gamma \ll \omega_0$ ($\gamma \rightarrow 0$), $\chi'' \sim \delta(\omega - \omega_0) - \delta(\omega + \omega_0)$ describes coherent propagating magnon excitations with $\omega_0 \approx \omega_1$ as a pole. The overdamped limit ($\gamma \approx \omega_0$), in contrast, is characterized by $\chi'' \propto \omega$ for $\omega \rightarrow 0$; see Fig. 1(b). Furthermore, for $\omega_0 > \omega_1$, neither of these two energy scales reflects the pole of a coherent excitation. However, as χ'' is broadly peaked at ω_1 , this energy scale is often referred to as the paramagnon excitation energy scale [12,20,38].

Fits to spectra taken at different momenta q along $q = (h, 0)$ and (h, h) are shown in Fig. 2. Solid lines indicate the elastic (blue) and low-energy excitation (red) contributions. In this fashion, γ , ω_0 , ω_1 , and χ_0'' were extracted for LSCO $x = 0.23$ along the two high-symmetry directions; see Figs. 3–5. From this analysis, it is found that $\gamma/2$ and ω_0 are comparable for all measured spectra. Interpreting the low-energy excitation along $(h, 0)$ as a spin excitation, as will be confirmed below, implies that it is overdamped. Along (h, h) , the nature of this excitation is less clear and probably has a mixed spin and charge

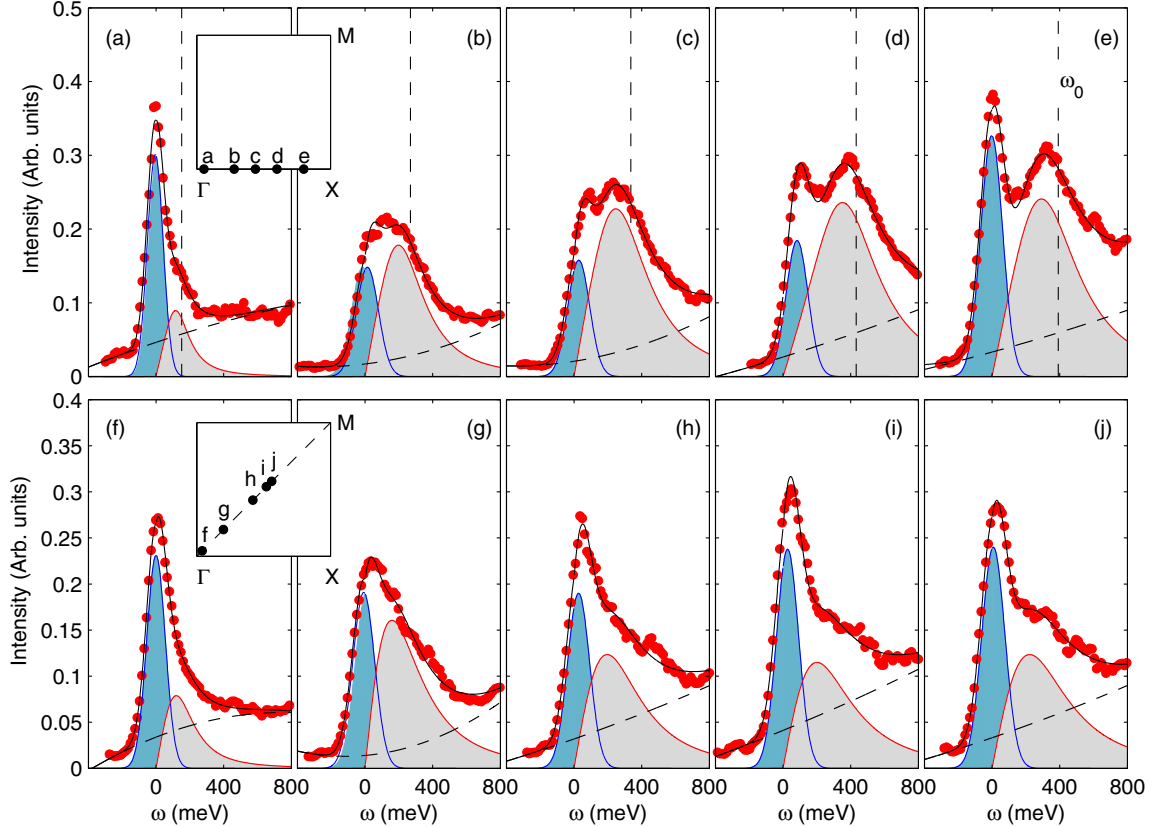


FIG. 2. RIXS spectra recorded on LSCO $x = 0.23$, at $T = 20$ K, in grazing incidence geometry using σ -polarized light tuned to the Cu L_3 edge (930 eV) line. (a)–(e) Spectra measured with momenta along $q = (h, 0)$ as indicated in the inset of (a). (f)–(j) Spectra taken along $q = (h, h)$ as indicated in the inset of (f) and (g). Blue and gray shaded areas are modeled contributions from elastic and low-energy excitations on top of a cubic background (dashed line). Solid black line is the sum of these contributions. See text for further explanation.

character, which makes the interpretation of its parameters more delicate. We note that the damping $\gamma/2$ softens upon moving from the zone boundary towards the zone center [Fig. 3(b)]. A similar angular dependence has previously been reported in optimally doped Ba_{0.6}K_{0.4}Fe₂As₂ [20] [reproduced in Fig. 3(a)]. Additionally, ω_0 disperses upward from the zone center and saturates near the zone boundary along both the $(h, 0)$ and (h, h) directions. A similar dispersion of ω_1 is found along $(h, 0)$. As $\gamma/2 \approx \omega_0$, along the nodal (h, h) direction, it is difficult to extract ω_1 reliably. Finally, we observe in Fig. 5 that the integrated intensity $\chi''_0 \cdot \gamma$ of the low-energy excitation is weakly but significantly anisotropic, as it is larger along the $(h, 0)$ direction than the (h, h) direction (for a given absolute value of the momentum $|q|$).

B. RPA susceptibility calculations

To analyze the RIXS intensities and neutron-scattering spectra, itinerant approaches have been applied [16,41–46]. These approaches are expected to be especially relevant for very overdoped cuprates, where the system enters a state with some of the characteristics of a Fermi liquid [33,47,48]. We have therefore calculated the random-phase approximation (RPA) spin susceptibility $\chi_s(\mathbf{q}, \omega)$ for overdoped LSCO to analyze the low-energy excitations in the paramagnetic state.

The RPA susceptibility describes the collective magnetic excitations of the itinerant electrons. Similar to Guarise *et al.* (Ref. [16]), here we obtain the transverse part of the spin susceptibility as

$$\chi_s(\mathbf{q}, \omega) = \frac{\chi_0(\mathbf{q}, \omega)}{1 - U\chi_0(\mathbf{q}, \omega)},$$

where $\chi_0(\mathbf{q}, \omega)$ represents the Lindhard response function [43] and U is the local Coulomb interaction. As input to χ_0 , we use the single-band tight-binding parametrization [49] of the electronic dispersion obtained from angle-resolved photoemission spectroscopy (ARPES) measurements on this sample [31]. The renormalized bandwidth $4t = 490$ meV was used and U is chosen to be $1.2t$, so that the susceptibility is not diverging, meaning that the system is far enough from a density-wave instability.

In fact, the RPA susceptibility χ_s induces moderate modifications of the particle-hole continuum obtained from the Lindhard response function χ_0 [see Fig. 6(a)]. Along $(\pi, 0)$, the dispersion in the particle-hole continuum is renormalized to lower energies (smaller bandwidth) and starts to develop a second branch, leading to a second minimum (softening) at around $(0.15, 0)$. In this sense, it can be interpreted as a spin excitation. Along (π, π) , the main changes occur around the M point, where low-energy spin excitations

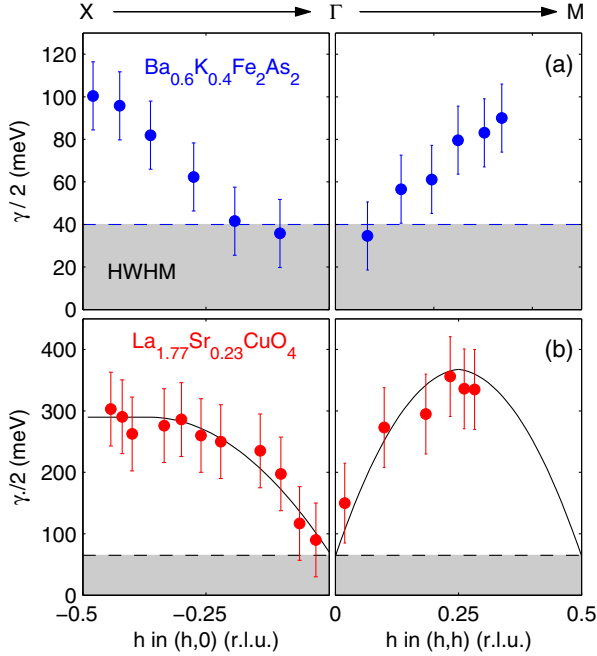


FIG. 3. Damping $\gamma/2$ (see text) of the low-energy excitations measured by RIXS in LSCO $x = 0.23$ (this work) and $Ba_{0.6}K_{0.4}Fe_2As_2$ [20] along the high-symmetry directions ΓX and ΓM . Error bars in the bottom panels are set by the applied energy resolution (65 meV—HWHM), which is also indicated by a horizontal dashed line.

near (π, π) are reproduced consistently with previous susceptibility calculations [44] (see the static Lindhard susceptibility in the inset of Fig. 4). Interestingly, a weakly dispersing branch is found in the range $(0,0) \rightarrow (0.2,0.2)$; see Figs. 6(a) and 6(c). As it gets stronger with increasing U , we interpret it as a spin-excitation branch. Notice, however, that after convolution of the applied instrumental resolution ($FWHM = 130$ meV), these detailed features are being smeared out completely [Figs. 6(b) and 6(e)].

V. DISCUSSION

The calculated RPA susceptibility contains contributions from both excited particle-hole continuum and spin excitations [16,45,46]. RIXS should be sensitive to both of these components. The convoluted RPA calculation reproduces the most salient observations. First, along the $(\pi,0)$ direction, the spectral weight distribution is reproduced quite successfully; compare Fig. 1(c) with Fig. 6(b). Moreover, the calculation also produces stronger damping as the excitations disperse towards the zone boundary. Second, the susceptibility calculation captures the intensity anisotropy between $(0,0) \rightarrow (\pi,0)$ and $(0,0) \rightarrow (\pi,\pi)$. Such a clear anisotropy in the intensity distribution (see Fig. 5) was not observed in the RIXS studies on doped cuprates in Refs. [16,27,39]. The susceptibility calculation, furthermore, makes a number of predictions that can be tested by improving the instrumental resolution. Most notable is the low-energy excitation branch along $(0,0) \rightarrow (\pi,\pi)$. Such a low-energy dispersion already appeared in the calculated RPA of other doped cuprates [16,27], but was not

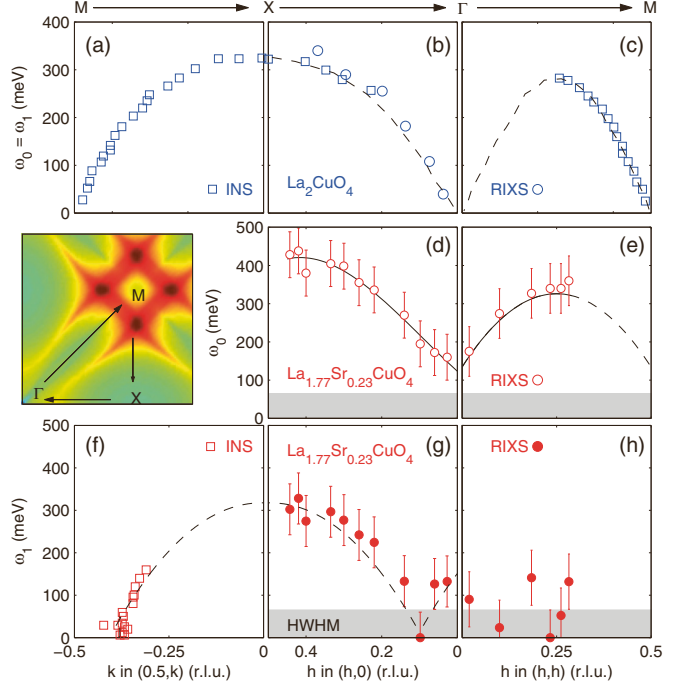


FIG. 4. Comparison of the spin-excitation dispersions ω_0 and ω_1 (see text) extracted on La_2CuO_4 (LCO) with the low-energy excitation dispersions on $La_{1.77}Sr_{0.23}CuO_4$ along high-symmetry directions as indicated. Data obtained from INS and RIXS are displayed by square and circular points, respectively. For LCO, good agreement between INS (□, Ref. [40]) and RIXS (○, Ref. [10]) is found along the ΓX direction. No overlap between RIXS (●, this work) and INS (□, Ref. [26]) has been reached for overdoped compositions of LSCO. The inset indicates the high-symmetry directions and displays the calculated static Lindhard susceptibility (for $\omega \rightarrow 0$) (see text for further explanation).

recognized as such, mainly because it was not as distinct as in the present case. We attribute its clear dispersive character here to the specific LSCO electronic structure that has a van Hove singularity in the antinodal region [31]. Improving the

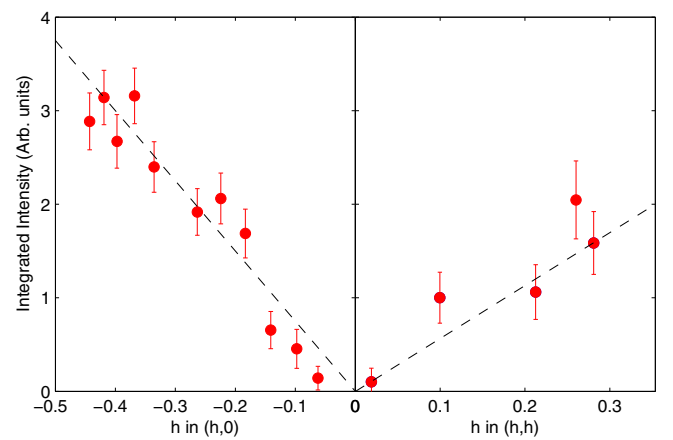


FIG. 5. Integrated intensity $\chi_0'' \cdot \gamma$ of the low-energy excitations measured by RIXS in LSCO $x = 0.23$ along the high-symmetry directions ΓX and ΓM . The dashed lines are a guide to the eyes.

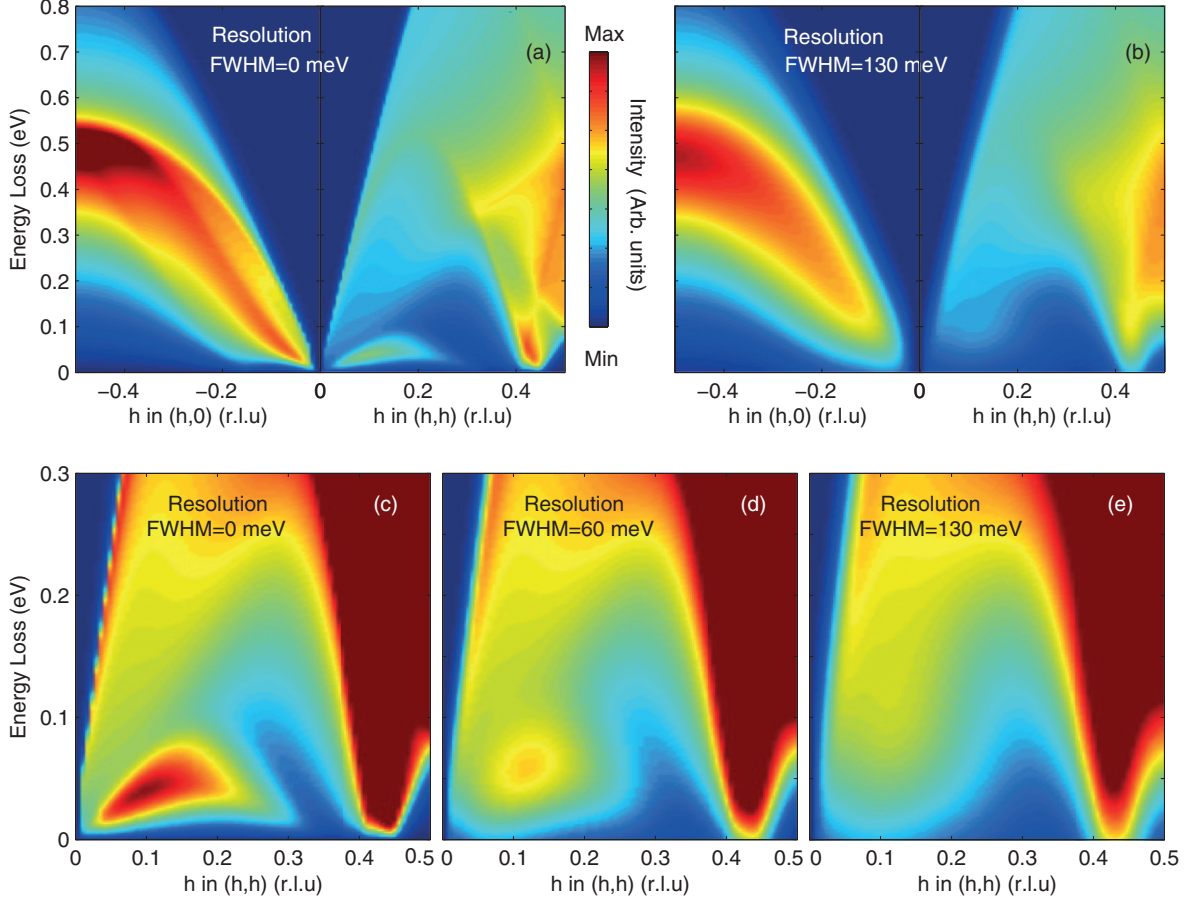


FIG. 6. (a) Calculated RPA susceptibility along the nodal (h,h) and antinodal direction $q = (h,0)$. (b) The RPA susceptibility convoluted by instrument resolution to make a direct comparison to Fig. 1(c). (c)–(e) A zoom of the low-energy nodal RPA susceptibility. In (d) and (e), a Gaussian convolution with FWHM = 60 and 130 meV has been applied. This demonstrates that a spectrometer with a FWHM = 60 meV energy resolution at the Cu L_3 edge is sufficient to test the RPA prediction of low-energy nodal spin excitations.

resolution to have a FWHM ~ 60 meV would be sufficient to resolve this predicted low-energy branch; see Fig. 6(d).

In comparison to the case of undoped cuprates [10,12], this analysis shows that the measured excitations in overdoped LSCO are, in general, broader and their width [see Fig. 3(b)] has a stronger momentum dependence. This most likely comes from the efficient damping of spin excitations by the electron-hole continuum, as well as from the contribution of electron-hole excitations to the RIXS signal [45,46].

We conclude the discussion by comparing RIXS and INS studies of LSCO [10,39]. For the undoped compound La_2CuO_4 , INS [40] and RIXS [10] experiments overlap along the ΓX direction and excellent agreement of the measured magnon dispersion is found (see Fig. 4). Neutron-scattering experiments on doped cuprates are typically restricted—due to weak cross sections—to a much narrower range around the $(0.5,0,0)$ point (indexed M) [26,50], where the so-called hour-glass spin-excitation dispersion is revealed [51–53]. The RIXS technique, on the other hand, has kinematic constraints limiting studies to a region centered around the Γ point. For doped cuprates, it is thus difficult to obtain a direct overlap of RIXS and INS spectra. Within the present RPA calculation, the Γ and M points are not equivalent. Caution should therefore

be taken when comparing neutron-scattering data near the M point with RIXS data recorded around the Γ point.

VI. CONCLUSIONS

In summary, we presented a Cu L_3 -edge RIXS study of the low-energy spin and charge excitations in overdoped $\text{La}_{1.77}\text{Sr}_{0.23}\text{CuO}_4$. Two high-symmetry directions $(h,0)$ and (h,h) were investigated. Spin excitations along (h,h) are strongly damped and the damping is displaying a significant momentum dependence—larger momentum yields larger damping. Spectral weight also has momentum dependence. Along the antinodal region, more spectral weight is found near the zone boundaries and more spectral weight is found in the antinodal direction than the nodal direction. RPA susceptibility calculations starting from the experimentally observed band structure capture these trends. This suggests that the measured RIXS signal originates from a mixture of spin excitations and a continuum of charge excitations. Furthermore, based on these calculations, we predict a low-energy dispersive spin-excitation branch, along the (π,π) direction, which is particularly intense and distinct from other features in the case of $\text{La}_{1.77}\text{Sr}_{0.23}\text{CuO}_4$. The emerging

ultrahigh-resolution spectrometers will be able to test this prediction.

ACKNOWLEDGMENTS

C.M., C.E.M., and J.C. acknowledge support by the Swiss National Science Foundation under Grants No. PZ00P2_154867, 200021-137783, No. PZ00P2_142434, and

No. BSSGI0_155873. C.M. also thanks the Alexander von Humboldt Foundation and MaNEP for financial support. S.M.H. acknowledges support by the United Kingdom Engineering and Physical Science Research Council under Grant No. EP/J015423/1. This work was performed at the ADRESS beam line of the SLS at the Paul Scherrer Institut, Villigen PSI, Switzerland. We thank the ADRESS beam-line staff for technical support.

- [1] J. Bardeen, L. N. Cooper, and J. R. Schrieffer, *Phys. Rev.* **108**, 1175 (1957).
- [2] T. Keller, P. Aynajian, K. Habicht, L. Boeri, S. K. Bose, and B. Keimer, *Phys. Rev. Lett.* **96**, 225501 (2006).
- [3] D. J. Scalapino, *Rev. Mod. Phys.* **84**, 1383 (2012).
- [4] R. J. Birgeneau, C. Stock, J. M. Tranquada, and K. Yamada, *J. Phys. Soc. Jpn.* **75**, 111003 (2006).
- [5] M. Fujita, H. Hiraka, M. Matsuda, M. Matsuura, J. M. Tranquada, S. Wakimoto, G. Xu, and K. Yamada, *J. Phys. Soc. Jpn.* **81**, 011007 (2012).
- [6] S. M. Hayden, G. Aeppli, H. A. Mook, T. G. Perring, T. E. Mason, S.-W. Cheong, and Z. Fisk, *Phys. Rev. Lett.* **76**, 1344 (1996).
- [7] L. J. P. Ament, M. van Veenendaal, T. P. Devereaux, J. P. Hill, and J. van den Brink, *Rev. Mod. Phys.* **83**, 705 (2011).
- [8] L. J. P. Ament, G. Ghiringhelli, M. M. Sala, L. Braicovich, and J. van den Brink, *Phys. Rev. Lett.* **103**, 117003 (2009).
- [9] L. Braicovich, L. J. P. Ament, V. Bisogni, F. Forte, C. Aruta, G. Balestrino, N. B. Brookes, G. M. De Luca, P. G. Medaglia, F. M. Granozio *et al.*, *Phys. Rev. Lett.* **102**, 167401 (2009).
- [10] L. Braicovich, J. van den Brink, V. Bisogni, M. M. Sala, L. J. P. Ament, N. B. Brookes, G. M. De Luca, M. Salluzzo, T. Schmitt, V. N. Strocov *et al.*, *Phys. Rev. Lett.* **104**, 077002 (2010).
- [11] J. Kim, D. Casa, M. H. Upton, T. Gog, Y.-J. Kim, J. F. Mitchell, M. van Veenendaal, M. Daghofer, J. van den Brink, G. Khaliullin *et al.*, *Phys. Rev. Lett.* **108**, 177003 (2012).
- [12] M. L. Tacon, G. Ghiringhelli, J. Chaloupka, M. M. Sala, V. Hinkov, M. W. Haverkort, M. Minola, M. Bakr, K. J. Zhou, S. Blanco-Canosa *et al.*, *Nat. Phys.* **7**, 725 (2011).
- [13] C. G. Fatuzzo, M. Dantz, S. Fatale, P. Olalde-Velasco, N. E. Shaik, B. Dalla Piazza, S. Toth, J. Pelliciari, R. Fittipaldi, A. Vecchione *et al.*, *Phys. Rev. B* **91**, 155104 (2015).
- [14] J. Schlappa, T. Schmitt, F. Vernay, V. N. Strocov, V. Ilakovac, B. Thielemann, H. M. Rønnow, S. Vanishri, A. Piazzalunga, X. Wang *et al.*, *Phys. Rev. Lett.* **103**, 047401 (2009).
- [15] J. Schlappa, K. Wohlfeld, K. J. Zhou, M. Mourigal, M. W. Haverkort, V. N. Strocov, L. Hozoi, C. Monney, S. Nishimoto, S. Singh *et al.*, *Nature (London)* **485**, 82 (2012).
- [16] M. Guarise, B. D. Piazza, H. Berger, E. Giannini, T. Schmitt, H. M. Rønnow, G. A. Sawatzky, J. van den Brink, D. Altenfeld, I. Eremin *et al.*, *Nat. Commun.* **5**, 5760 (2014).
- [17] B. Dalla Piazza, M. Mourigal, M. Guarise, H. Berger, T. Schmitt, K. J. Zhou, M. Grioni, and H. M. Rønnow, *Phys. Rev. B* **85**, 100508 (2012).
- [18] M. Guarise, B. Dalla Piazza, M. Moretti Sala, G. Ghiringhelli, L. Braicovich, H. Berger, J. N. Hancock, D. van der Marel, T. Schmitt, V. N. Strocov *et al.*, *Phys. Rev. Lett.* **105**, 157006 (2010).
- [19] M. Minola, G. Dellea, H. Gretarsson, Y. Peng, Y. Lu, J. Porras, T. Loew, F. Yakhou, N. Brookes, Y. Huang *et al.*, *Phys. Rev. Lett.* **114**, 217003 (2015).
- [20] K.-J. Zhou, Y.-B. Huang, C. Monney, X. Dai, V. N. Strocov, N.-L. Wang, Z.-G. Chen, C. Zhang, P. Dai, L. Patthey *et al.*, *Nat. Comm.* **4**, 1470 (2013).
- [21] M. P. M. Dean, G. Dellea, R. S. Springell, F. Yakhou-Harris, K. Kummer, N. B. Brookes, X. Liu, Y.-J. Sun, J. Strle, T. Schmitt *et al.*, *Nat. Mater.* **12**, 1019 (2013).
- [22] H. Kimura, M. Kofu, Y. Matsumoto, and K. Hirota, *Phys. Rev. Lett.* **91**, 067002 (2003).
- [23] J. Chang, A. P. Schnyder, R. Gilardi, H. M. Rønnow, S. Pailhes, N. B. Christensen, C. Niedermayer, D. F. McMorrow, A. Hiess, A. Stunault *et al.*, *Phys. Rev. Lett.* **98**, 077004 (2007).
- [24] J. Chang, N. B. Christensen, C. Niedermayer, K. Lefmann, H. M. Rønnow, D. F. McMorrow, A. Schneidewind, P. Link, A. Hiess, M. Boehm *et al.*, *Phys. Rev. Lett.* **102**, 177006 (2009).
- [25] B. Vignolle, S. M. Hayden, D. F. McMorrow, H. M. Rønnow, B. Lake, C. D. Frost, and T. G. Perring, *Nat. Phys.* **3**, 163 (2007).
- [26] O. J. Lipscombe, S. M. Hayden, B. Vignolle, D. F. McMorrow, and T. G. Perring, *Phys. Rev. Lett.* **99**, 067002 (2007).
- [27] M. P. M. Dean, A. J. A. James, A. C. Walters, V. Bisogni, I. Jarrige, M. Hücker, E. Giannini, M. Fujita, J. Pelliciari, Y. B. Huang *et al.*, *Phys. Rev. B* **90**, 220506 (2014).
- [28] M. P. M. Dean, A. J. A. James, R. S. Springell, X. Liu, C. Monney, K. J. Zhou, R. M. Konik, J. S. Wen, Z. J. Xu, G. D. Gu *et al.*, *Phys. Rev. Lett.* **110**, 147001 (2013).
- [29] G. Ghiringhelli, A. Piazzalunga, C. Dallera, G. Trezzi, L. Braicovich, T. Schmitt, V. N. Strocov, R. Betemps, L. Patthey, X. Wang *et al.*, *Rev. Sci. Instrum.* **77**, 113108 (2006).
- [30] V. N. Strocov, T. Schmitt, U. Flechsig, T. Schmidt, A. Imhof, Q. Chen, J. Raabe, R. Betemps, D. Zimoch, J. Krempasky *et al.*, *J. Synchrotron Radiat.* **17**, 631 (2010).
- [31] J. J. Chang, M. Måansson, S. Pailhès, T. Claesson, O. J. Lipscombe, S. M. Hayden, L. Patthey, O. Tjernberg, and J. Mesot, *Nat. Commun.* **4**, 2559 (2013).
- [32] J. Chang, J. S. White, M. Laver, C. J. Bowell, S. P. Brown, A. T. Holmes, L. Maechler, S. Strässle, R. Gilardi, S. Gerber *et al.*, *Phys. Rev. B* **85**, 134520 (2012).
- [33] C. G. Fatuzzo, Y. Sassa, M. Måansson, S. Pailhès, O. J. Lipscombe, S. M. Hayden, L. Patthey, M. Shi, M. Grioni, H. M. Rønnow *et al.*, *Phys. Rev. B* **89**, 205104 (2014).
- [34] S. Komiya, Y. Ando, X. F. Sun, and A. N. Lavrov, *Phys. Rev. B* **65**, 214535 (2002).
- [35] G. Ghiringhelli, N. B. Brookes, E. Annese, H. Berger, C. Dallera, M. Grioni, L. Perfetti, A. Tagliaferri, and L. Braicovich, *Phys. Rev. Lett.* **92**, 117406 (2004).

- [36] M. M. Sala, V. Bisogni, C. Aruta, G. Balestrino, H. Berger, N. B. Brookes, G. M. de Luca, D. D. Castro, M. Grioni, M. Guarise *et al.*, *New J. Phys.* **13**, 043026 (2011).
- [37] M. van Veenendaal, *Phys. Rev. Lett.* **96**, 117404 (2006).
- [38] M. Le Tacon, M. Minola, D. C. Peets, M. Moretti Sala, S. Blanco-Canosa, V. Hinkov, R. Liang, D. A. Bonn, W. N. Hardy, C. T. Lin *et al.*, *Phys. Rev. B* **88**, 020501 (2013).
- [39] S. Wakimoto, K. Ishii, H. Kimura, M. Fujita, G. Dellea, K. Kummer, L. Braicovich, G. Ghiringhelli, L. M. Debeer-Schmitt, and G. E. Granroth, *Phys. Rev. B* **91**, 184513 (2015).
- [40] N. S. Headings, S. M. Hayden, R. Coldea, and T. G. Perring, *Phys. Rev. Lett.* **105**, 247001 (2010).
- [41] W. Chen and O. P. Sushkov, *Phys. Rev. B* **88**, 184501 (2013).
- [42] M. R. Norman, *Phys. Rev. B* **63**, 092509 (2001).
- [43] I. Eremin and D. Manske, *Phys. Rev. Lett.* **94**, 067006 (2005).
- [44] R.-H. He, M. Fujita, M. Enoki, M. Hashimoto, S. Iikubo, S.-K. Mo, H. Yao, T. Adachi, Y. Koike, Z. Hussain *et al.*, *Phys. Rev. Lett.* **107**, 127002 (2011).
- [45] D. Benjamin, I. Klich, and E. Demler, *Phys. Rev. Lett.* **112**, 247002 (2014).
- [46] R. Zeyher and A. Greco, *Phys. Rev. B* **87**, 224511 (2013).
- [47] S. Nakamae, K. Behnia, N. Mangkorntong, M. Nohara, H. Takagi, S. J. C. Yates, and N. E. Hussey, *Phys. Rev. B* **68**, 100502(R) (2003).
- [48] B. Vignolle, A. Carrington, R. A. Cooper, M. M. J. French, A. P. Mackenzie, C. Jaudet, D. Vignolles, C. Proust, and N. E. Hussey, *Nature (London)* **455**, 952 (2008).
- [49] E. Pavarini, I. Dasgupta, T. Saha-Dasgupta, O. Jepsen, and O. K. Andersen, *Phys. Rev. Lett.* **87**, 047003 (2001).
- [50] S. Wakimoto, K. Yamada, J. M. Tranquada, C. D. Frost, R. J. Birgeneau, and H. Zhang, *Phys. Rev. Lett.* **98**, 247003 (2007).
- [51] S. M. Hayden, H. A. Mook, P. Dai, T. G. Perring, and F. Dogan, *Nature (London)* **429**, 531 (2004).
- [52] J. M. Tranquada, H. Woo, T. G. Perring, H. Goka, G. D. Gu, G. Xu, M. Fujita, and K. Yamada, *Nature (London)* **429**, 534 (2004).
- [53] N. B. Christensen, D. F. McMorrow, H. M. Rønnow, B. Lake, S. M. Hayden, G. Aeppli, T. G. Perring, M. Mangkorntong, M. Nohara, and H. Tagaki, *Phys. Rev. Lett.* **93**, 147002 (2004).